

Emergence of multistrain epidemics with an underlying genotype network

Blake J. M. Williams¹, Guillaume St-Onge^{2,3}, and Laurent Hébert-Dufresne^{1,2,4,*}

¹Vermont Complex Systems Center, University of Vermont, Burlington, VT 05405, USA

²Département de physique, de génie physique et d'optique, Université Laval, Québec (Québec), Canada G1V 0A6

³Centre interdisciplinaire en modélisation mathématique, Université Laval, Québec (Québec), Canada G1V 0A6

⁴Department of Computer Science, University of Vermont, Burlington, VT 05405, USA

*laurent.hebert-dufresne@uvm.edu

ABSTRACT

Mathematical disease modeling has long operated under the assumption that any one infectious disease is caused by one transmissible pathogen spreading among a population. This paradigm has been useful in simplifying the biological reality of epidemics and has allowed the modeling community to focus on the complexity of other factors such as population structure and interventions. However, there is an increasing amount of evidence that the strain diversity of pathogens, and their interplay with the host immune system, can play a large role in shaping the dynamics of epidemics. Here, we introduce a disease model with an underlying genotype network to account for two important mechanisms. One, the disease can mutate along network pathways as it spreads in a host population. Two, the genotype network allows us to define a genetic distance across strains and therefore to model the transcendence of immunity often observed in real world pathogens. We study the emergence of epidemics in this model, through its epidemic phase transitions, and highlight the role of the genotype network in driving cyclicity of diseases, large scale fluctuations, sequential epidemic transitions, as well as localization around specific strains of the associated pathogen. More generally, our model illustrates the richness of behaviors that are possible even in well-mixed host populations once we consider strain diversity and go beyond the “one disease equals one pathogen” paradigm.

1 Introduction

Viral species are known to often undergo rapid evolution. Since the early 20th century, influenza viruses have been described as having marked variability and unpredictable behavior¹. Subsequent RNA virus studies of the 20th and 21st century have focused on, among others, the *Zaire ebolavirus*, strains of the SARS-CoV species, and HIV-1, all possessing high mutation rates². These frequent mutations contribute to the antigenic evolution of these viruses, allowing them to evade recognition by the human immune system³.

Despite the long-standing knowledge of subtypes and strains within viral species, mathematical disease modeling has continued to model viral diseases with one underlying pathogen. Notably, influenza violates the “one disease, one pathogen” paradigm: numerous types, subtypes, and strains of influenza viruses challenge the human immune system, driving vaccine effectiveness below 50% in most recent years⁴⁻⁷. Models which fail to account for antigenic variation of a pathogen may lead to biased characterizations of epidemic emergence and progression.

Modeling multi-strain pathogens with consideration for antigenic properties requires the inclusion of cross-protective effects, in which the immunity acquired towards one strain offers partial protection towards another strain based on their antigenic similarity. Cross-protection is seen in numerous viral species⁸⁻¹⁰. In general, more similar strains will have greater cross-protective effects, as with seasonal influenza¹¹. However, cross-protective immunity is not necessarily a monotonically decreasing function of antigenic distance. Antibody-dependent enhancement has been observed in dengue viruses, in which a past infection may in fact increase the risk of severe infection^{12,13}. Regardless, approximations of cross-protection may be made through antigenic distance or genetic distance. This relationship may be determined by a function of genetic distance to approximate the unique antigenic distances between all strains.

Several models have been proposed in the growing sub-discipline of multistrain disease modeling¹⁴. These models balance biological assumptions with computational tractability through reduction via symmetry (e.g. antigenic neighborhoods¹⁵) age structure¹⁶, and deciding to capture either infection history or immune status¹⁴ among other modeling choices. Cross-protective immunity has been explored in two-strain models¹⁷, multi-strain models with a restricted number of antigenic loci and alleles¹⁸, and temporary cross-protective immunity in dengue models¹⁹ capable of producing cyclical and chaos-like infection progression. However, the effects of an underlying genotype network structure — governing viable mutation pathways and genetic distances between strains — have not been thoroughly explored with multistrain models. Genotype networks consist of nodes that

represent strains, with edges connecting strains that differ by one nucleotide or amino acid in some antigenic region of a gene or protein²⁰. Genotype networks are a complementary structure to phylogenetic trees, and are a useful way of representing genetic distance necessary for cross-immunity in multi-strain models.

Moreover, the genotype network gives us a proxy through which we can specify potential mutation pathways between strains. Mechanisms for pathogen mutation have previously been included in mathematical models^{21,22}, often to consider the emergence of antiviral resistance^{23–26}. Particularly, these models predict the emergence of sequential epidemic transitions — with a first epidemic threshold defining the emergence of macroscopic disease spread and a second marking the emergence of treatment resistant strain²⁴. However, such models are often limited to only two pathogen strains as they require specification of the fitness cost associated with resistance. We therefore aim to introduce a more general model, allowing large number of strains to mutate along specific network pathways. While this general model could consider a complex fitness landscape over this genotype network, we focus on the case of neutral evolution and show how the previous results discussed here can all co-exist within a single, fairly simple, model.

We introduce a multistrain Susceptible-Infectious-Recovered-Susceptible (multistrain SIRS) epidemic model with an underlying genotype network, allowing the disease to evolve along plausible mutation pathways as it spreads in a well-mixed population. We then investigate the effects of genotype network structure on the emergence of an endemic state and on the fitness distribution of strains across the genotype network. Altogether, our results challenge the typical phenomenology of epidemic models. We find two epidemic transitions: one marking the emergence of an endemic state driven by a subset of strains well localized on the genotype network and one marking a delocalization on the network, where all strains now contribute to the endemic strain. Between these thresholds, we find chaos-like behavior which can be maintained for arbitrarily long times, yielding time series with epidemic cycles featuring large unpredictable fluctuations.

2 Model

We study the spread on infectious disease within a well-mixed population for a defined genotype network of the chosen pathogen. Our model is as follows.

The underlying epidemiological dynamics correspond to a simple SIRS model, but where we add a genotype network defined as a set of potential mutations, meaning an infection of strain $i \in [1, N]$ can mutate along the network to a neighbouring strain $j \in \mathcal{N}_i$, where \mathcal{N}_i specifies the set of first network neighbours of strain i . Biologically, this network is defined such that neighbouring strains i and j differ by one unit of genetic distance.

The strains spread within a well-mixed host population. Host individuals are defined as susceptible (S) if they possess no immunity to any strain of a disease, see Fig. 1. Susceptible individuals progress to infectious state I_i at transmission rate β for every contact with individuals infectious with strain i , occurring at rate βI_i for every susceptible individual. Note that this basic transmission rate is held constant for all strains, as we focus on neutral evolution as a first approximation.

Individuals in I_i can either: (i) recover at rate γ to state R_i and acquire direct immunity for strain i and partial immunity to strain $j \neq i$; or (ii) become infected with strain I_j via mutation at a rate μ for all strains j in \mathcal{N}_i . Individuals in R_i will either: (i) lose immunity and progress to S at rate α , or (ii) become infected with strain $j \neq i$ to which they only possessed partial immunity and progress to I_j at a reduced rate β^* , where β^* is an exponentially decaying function of genetic distance between strains i, j . Specifically:

$$\beta^* \propto 1 - e^{-x_{ij}/\Delta} \quad (1)$$

where x_{ij} is the genetic distance between strain i, j (approximated by shortest path of length $x_{ij} = x_{ji}$ between strains i, j in the genotype network) and Δ is the rate of immunity transcendence ($0 < \Delta < \infty$).

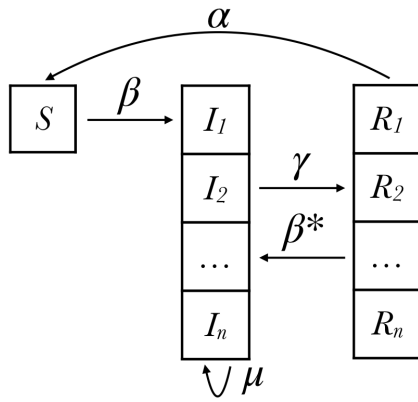
Altogether, the dynamics of our model can be followed by the following set of ordinary differential equations (ODEs),

$$\frac{dS}{dt} = -\beta \sum_{i=1}^N \frac{S I_i}{N} + \alpha \sum_{i=1}^N R_i \quad (2)$$

$$\frac{dI_i}{dt} = \beta \frac{S I_i}{N} - \gamma I_i + \mu \sum_{j=1}^N A_{i,j} (I_j - I_i) + \beta \sum_{j=1}^N \left(1 - e^{-x_{ij}/\Delta}\right) \frac{I_j R_j}{N} \quad (3)$$

$$\frac{dR_i}{dt} = \gamma I_i - \alpha R_i - \beta \sum_{j=1}^N \left(1 - e^{-x_{ij}/\Delta}\right) \frac{I_j R_i}{N} \quad (4)$$

where A_{ij} is an element of the adjacency matrix of the genotype network, equal to 1 if there is mutation pathway between i and j and 0 otherwise.



Symbol	Parameter
n	# strains
N	population size
S	susceptible
I_i	infected (strain i)
R_i	recovered (strain i)
β	transmission rate
γ	recovery rate
α	immunity loss rate
μ	mutation rate
Δ	characteristic length of immunity transcendence
A	adjacency matrix of the genotype network
x_{ij}	shortest path length between strains i & j

Figure 1. Compartmental model of a multistrain epidemic with an underlying genotype network (**left**), with parameters (**right**).

We therefore have 5 important epidemiological parameters: transmission rate β , recovery rate γ , rate of waning immunity α , mutation rate μ and immunity transcendence Δ . Unless mentioned otherwise, we typically fix the recovery rate $\gamma = 1$ such that other rates are defined in units of infectious period (and Δ in units of genetic distance). The other parameters then allow us to investigate different interesting regimes,

As $\Delta \rightarrow 0$, immunity becomes strain specific with no cross-protective effects. As $\Delta \rightarrow \infty$, immunity becomes broad-reaching to the point of universal protection across all strains. With β^* as a function of distance, we are able to reduce model complexity by avoiding specification of β_{ij}^* among all strains, whose values may not be known in real-world applications. Instead, we rely on the inverse relationship between antigenic distance and cross-protection that has been observed in influenza viruses¹¹. Note that this relationship may not be monotonically decreasing for all pathogens, in which case β^* may be defined by a function of genetic distance unique to the pathogens.

Our most important assumption is perhaps that only the most recent infection is relevant for cross-immunity effects. Indeed, I_i and R_i specify the pathogen involved only in the most recent infection for every individual. The alternative would have been to model an infectious state $I_{i,j,\dots}$ for all unique infection histories, of complexity $\mathcal{O}(2^n)$ if order does not matter and complexity $\mathcal{O}(n!)$ if it does. While a big assumption, focusing on the most recent infection reduces the complexity to $\mathcal{O}(n)$. Computational feasibility would be largely restricted, which would limit the analysis of the effects of genotype network structure^{14,27}. The infection history approximation enables genotype networks to be large enough to contain complex structure, necessary to investigate the role of genotype networks in epidemic progression.

3 Results

We focus our attention on the consequences of the genotype network underlying the spread of the disease. In order to gain as much insights as possible on how it affect prevalence of a disease, we keep the network itself simple using well-known graph toy models composed of lattices, chains and stars.

3.1 Localization in genotype space

We first ask which strains can be expected to have an advantage, not because of their own fitness or of our epidemiological parameters (as they all share the same β , γ and α), but because of their position in the genotype network. We use three simple network structures — a star, a square lattice, and a chain, all containing 25 strains — and run our model to produce a large outbreak with $\beta = 25$ much greater than the expected SIRS epidemics threshold of $\beta_c = 1$. Accordingly, we set the evolutionary dynamics to be much slower than that of epidemic spread with $\mu = 10^{-3}$. We then let the system reach its endemic steady state, where the derivatives in Eqs. (2-4) essentially go to zero such that the system is at equilibrium.

We observe a localization of infections by strain within genotype networks as shown in Fig. 2, top row. Stationary or endemic infection counts I_i^* differ from strain to strain, even with the assumption of neutral evolution, based solely on their position in the network and the resulting cross-protective immune effects. Epidemics can therefore be localized around a minority of strains, as is clear in the lattice and chain networks.

We quantify this localization phenomena with Kish's effective sample size²⁸, referred to here as effective participation ratio $n_{eff}^* = n_{eff}/n$. As $n_{eff}^* \rightarrow 1$, all strains contribute an equal number of infections. As $n_{eff}^* \rightarrow n^{-1}$, only one strain contributes infections. In Fig. 2, top row, we observe lower n_{eff}^* in the lattice and chain, indicating greater localization. A small number of

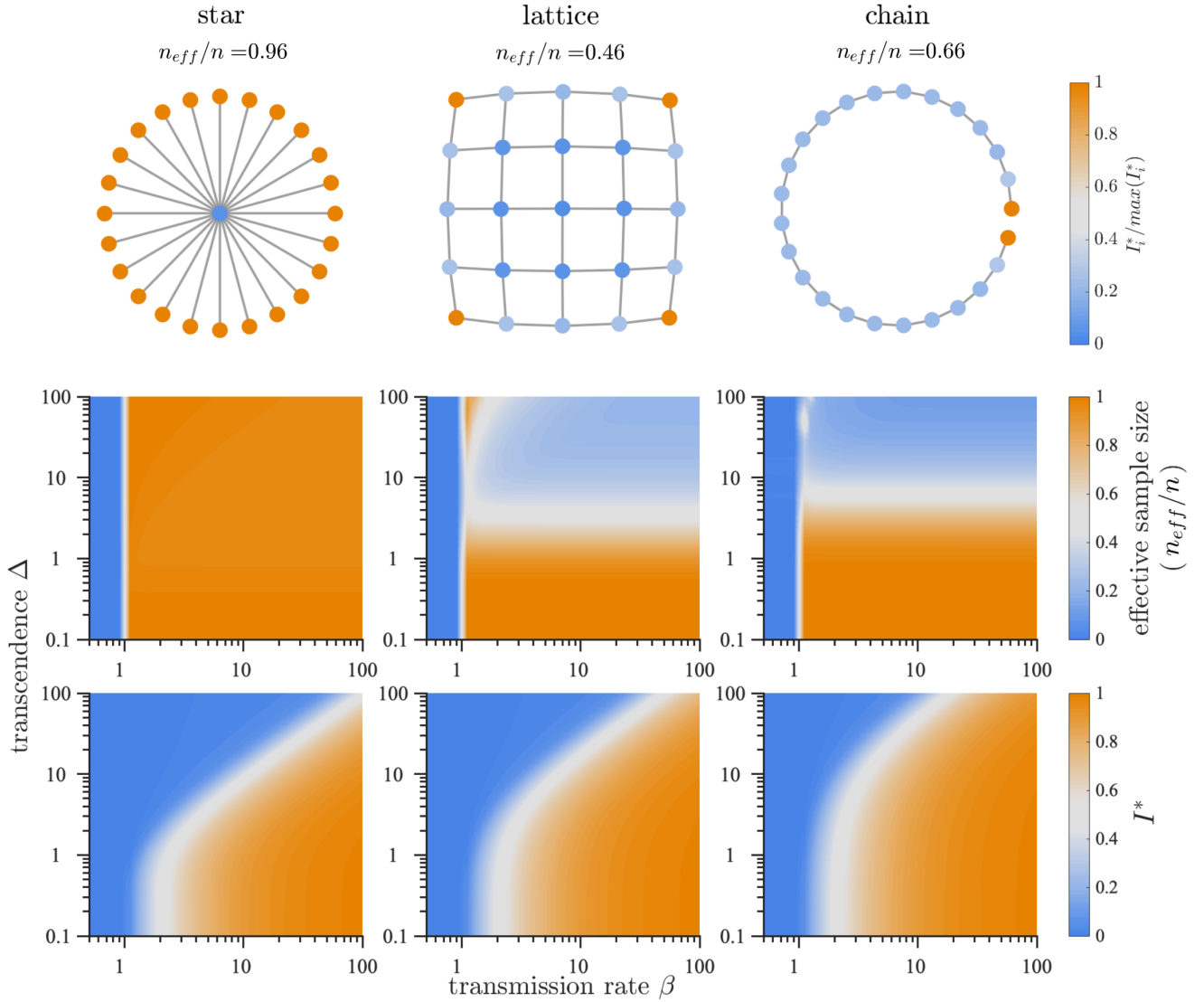


Figure 2. Infection localization and characteristics of endemic infection state. **(Top)** Localization within networks shown by endemic infection counts I_i^* normalized by $\max(I_i^*)$ for a given network. We use mutation rate $\mu = 10^{-3}$, transmission rate $\beta = 25$, waning immunity rate $\alpha = 1/50$, and transcending immunity $\Delta = 4$. **(Middle)** Infection localization regimes are revealed where normalized effective sample size is low (lattice and chain), occurring when few strains account for the majority of infections. **(Bottom)** endemic infections depend on not only transmission rate β , but also the breadth of cross-protective effects determined by transience rate Δ . Fixed parameters are $n = 25$, $\mu = 10^{-3}$, $\alpha = 1/50$.

strains are able to escape strong cross-protective immunity in the corners of the lattice and at the ends of the chain, while such heterogeneity is not seen in the star and ring networks.

As network structure determines infection localization, so does the transience of immunity. In Fig. 2, middle row, we see n_{eff}^* as a function of β and immunity transience Δ , revealing regimes of strong localization in the lattice and chain networks where n_{eff}^* remains small. High values of $\Delta > 10$, indicating far-reaching cross-protection, are associated with localization in these two networks. The structure of the star and loop networks allow them to escape localization effects influenced by large Δ .

Stationary infection counts I^* are also influenced by immunity transience Δ . In Fig. 2, bottom row, we see reductions in I^* as Δ increases. As cross-protective effects increase, a higher β becomes necessary to maintain infections. Again we see the importance of network structure, with different values of Δ required between networks to affect I^* .

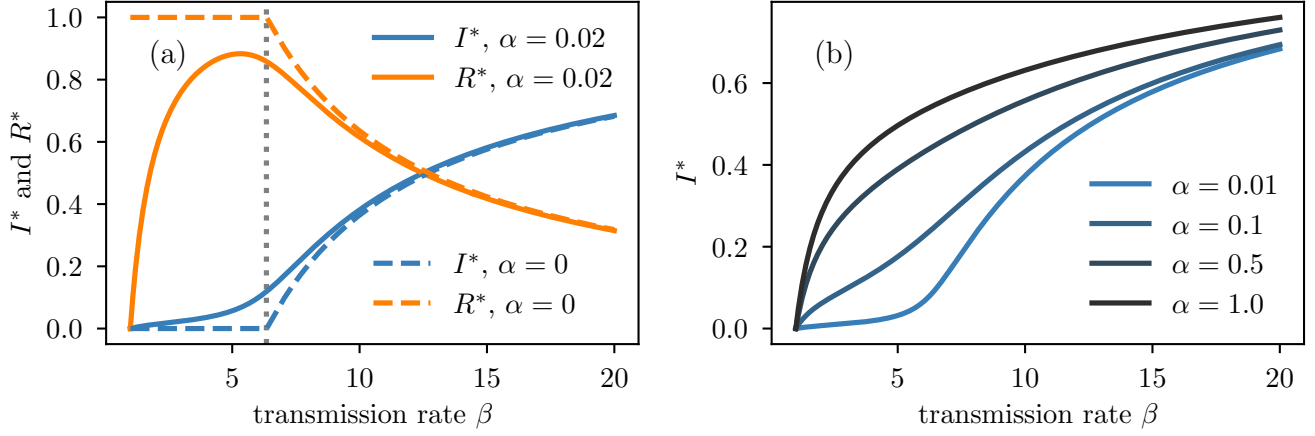


Figure 3. Bifurcation diagram for the model with varying levels of waning immunity on a star genotype network with 10 strains. We fix the recovery rate to $\gamma = 1$, the mutation rate $\mu = 1/100$, the transcending immunity $\Delta = 10$ and we vary the transmission rate β . **(Left)** We set the waning immunity rate $\alpha \in \{0, 0.02\}$ to illustrate the origin of the immune invasion threshold (vertical dotted line) obtained with Eqs. (5) and (6). **(Right)** For large enough values of waning immunity rate, the immune invasion threshold disappears.

3.2 Sequential phase transitions

We then look at the behaviour of the endemic state as we vary the basic transmission rate β . We know from classic SIRS model that there should be an epidemic transition at $\beta_c = 1$, marking a transition between a disease-free phase where the disease is too weak to establish itself in the population if $\beta < 1$, and an endemic phase for larger values. Yet, one interesting result of Fig. 2, bottom row is that the epidemic threshold now seem to increase with transcending immunity Δ . This is somewhat surprising given that Δ does not matter for any one strain, which should still be able to survive on its own following SIRS dynamics once $\beta > \beta_c = 1$.

In Fig. 3, we take a deeper look at the phase diagram under varying transmission rate and observe a *second* epidemic transition. More precisely, I^* is no longer a concave function of transmission rate; it emerges as expected at $\beta_c = 1$ but has a new inflection point at a much higher β value. This means that only modest increases in I^* are seen when β is just above to the epidemic threshold $\beta_c = 1$, in contrast to standard SIS-like models in which this regime experiences the most rapid rate of change in I^* as a function of β ²⁹.

We conjecture that this second phase transition is governed by what we call the *immune invasion threshold*, corresponding to the point at which infected nodes starts to infect recovered nodes (of other strains) effectively. To see this, in Fig. 3, we compare the bifurcation diagrams of two models: with and without waning immunity. In the latter case, in the stationary state, a node infected with strain i can only infect recovered nodes of strains $j \neq i$ (since $S^* = 0$). The immune invasion threshold β_I can thus be estimated from β_c if $\alpha \mapsto 0$. Surprisingly, even though $\beta_c = 1$ whenever $\alpha > 0$, it is no longer the case when $\alpha = 0$.

To derive the immune invasion threshold, let us rewrite the stationary state quantities I^*, R^* when $\alpha = 0$. We have

$$\begin{aligned} 0 &= -\gamma I_i^* + \mu \sum_j A_{ij} I_j^* - \mu k_i + \beta I_i^* \sum_j T_{ij} R_j^*, \\ 0 &= \gamma I_i^* - \beta R_i^* \sum_j T_{ij} I_j^*, \end{aligned}$$

where $T_{ij} \equiv (1 - e^{-x_{ij}/\Delta})$. Isolating R_i^* in the second equation and reinjecting the solution in the first one, we obtain a self-consistent equation for the $\{I_i^*\}$,

$$I_i^* = \frac{\sum_j A_{ij} I_j^*}{\frac{\gamma}{\mu} \left(1 - \sum_j T_{ij} \frac{I_j^*}{\sum_k T_{jk} I_k^*}\right) + k_i}. \quad (5)$$

Interestingly, the $\{I_i^*\}$ do not depend upon β . However, we know that such solution is possible only if $I_i^* > 0 \forall i$, and this break down at β_I when $R^* = \sum_i R_i^* \rightarrow 1$. Therefore, the immune invasion threshold β_I has the following explicit expression

$$\beta_I = \gamma \sum_i \frac{I_i^*}{\sum_j T_{ij} I_j^*}, \quad (6)$$

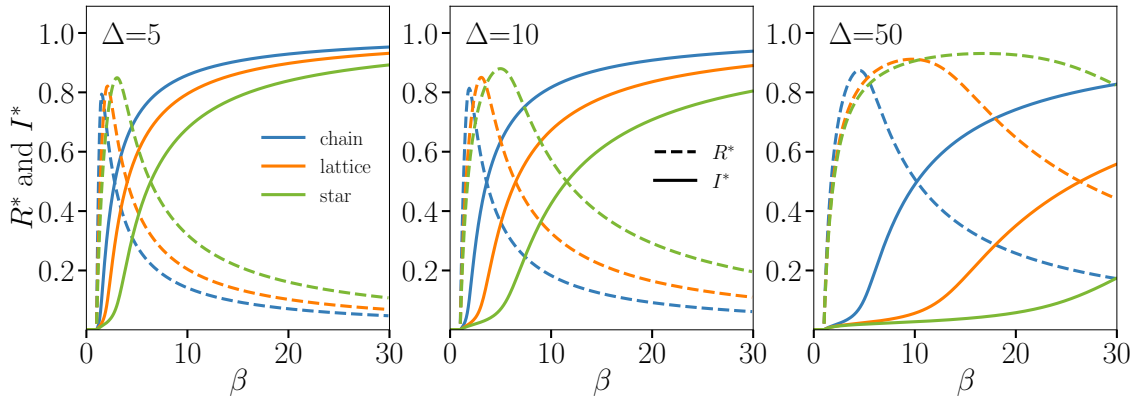


Figure 4. Integration of the ODEs on three toy genotype networks — the chain, square lattice and star — all with 25 strains. We fix the recovery rate $\gamma = 1$, the mutation rate $\mu = 1/100$, the waning immunity rate $\alpha = 1/50$ and vary the transmission rate β under three values of transcending immunity: (a) $\Delta = 5$, (b) $\Delta = 10$, (c) $\Delta = 50$. Close to the inflection point of every I^* curve (shown in solid lines) we find a maximum in R^* (shown in dashed lines). This point therefore marks a second activation threshold, one where the transmission rate is high enough to counteract transcending immunity and spread the outbreak using the pool of recovered individuals.

where the $\{I_i^*\}$ are evaluated from Eq. (5).

We observe a direct relationship between Δ and β_I . Namely, when $\Delta \rightarrow \infty$, $T_{ij} \rightarrow 0$ for all i, j , hence $\beta_I \rightarrow \infty$, as seen from Eq. (6). When $\Delta \rightarrow 0$, $T_{ij} \rightarrow 1$ for all $i \neq j$, and $T_{ii} = 0$, hence

$$\beta_I \rightarrow \gamma \sum_i \frac{I_i^*}{\sum_{j \neq i} I_j^*}.$$

For large networks, $\beta_I \approx \gamma \equiv 1$ in the limit $\Delta \rightarrow 0$. Therefore, we conclude that increasing Δ increases the immune invasion threshold, which makes sense based on intuition alone.

This relationship is shown in Fig. 4 for the three toy networks across multiple values of Δ . As Δ increases, immunity becomes wide-reaching in genetic distance, approaching the effects of universal immunity or a universal vaccine. This has the effect of necessitating higher β to produce the same I^* as lower values of Δ . Importantly, because of the sum in the denominator of Eq. (6), the immune invasion threshold β_I is not simply set by the diameter of the genotype network (i.e., the maximum value of x_{ij}), and is instead set by the entire network structure. While strains maximally distant from each other can of course better infect recovered individuals, competition between strains also play an important role: central strains can still infect individuals and grant them better immunity due to their central position in the network. Thus, the network structure plays a nontrivial role in setting the exact value of β_I as determined by Eq. (6).

3.3 Rich dynamics in between epidemic thresholds

Beyond the features of the endemic state, we observe rich prevalence dynamics throughout the epidemic when transmission rates are between the epidemic threshold $\beta_c = 1$ and the immune invasion threshold $\beta_I \geq \beta_c$. By comparing the top, middle, and bottom rows of Fig. 5 we see infection counts throughout the epidemic simulation while the transmission rate lays in different regimes, decreasing from $\beta > \beta_I$ to values closer to $\beta_c = 1$.

For transmission rate below the immune invasion threshold (bottom two rows), we see oscillations in the overall infection counts across all three networks before converging on an endemic value, resembling a dampened pseudo-chaotic behavior. Noting the different time scales shown, the chain rapidly converges on its endemic state while the star undergoes drastic oscillations before convergence. We see variation in infection counts at the strain level, with the infection counts for 3 of the 25 strains shown. At the strain level we see convergence occurring on different time scales within the same network, as well as variability in oscillatory nature.

In comparison, the top row of Fig. 5 shows the rapid convergence on the endemic state when the transmission rate is high ($\beta = 25$). There still exists infection localization, as indicated by different endemic infection counts at the strain level, as well as variability in convergence time between strains. However, the oscillatory nature is profoundly absent at transmission rates well about β_I . In contrast, as transmission rates are lowered towards $\beta_c = 1$ in the bottom rows of Fig. 5, we see the oscillations preserved but stretched across a broader timescale. Importantly, as the timescale of oscillations is stretched, their minimal

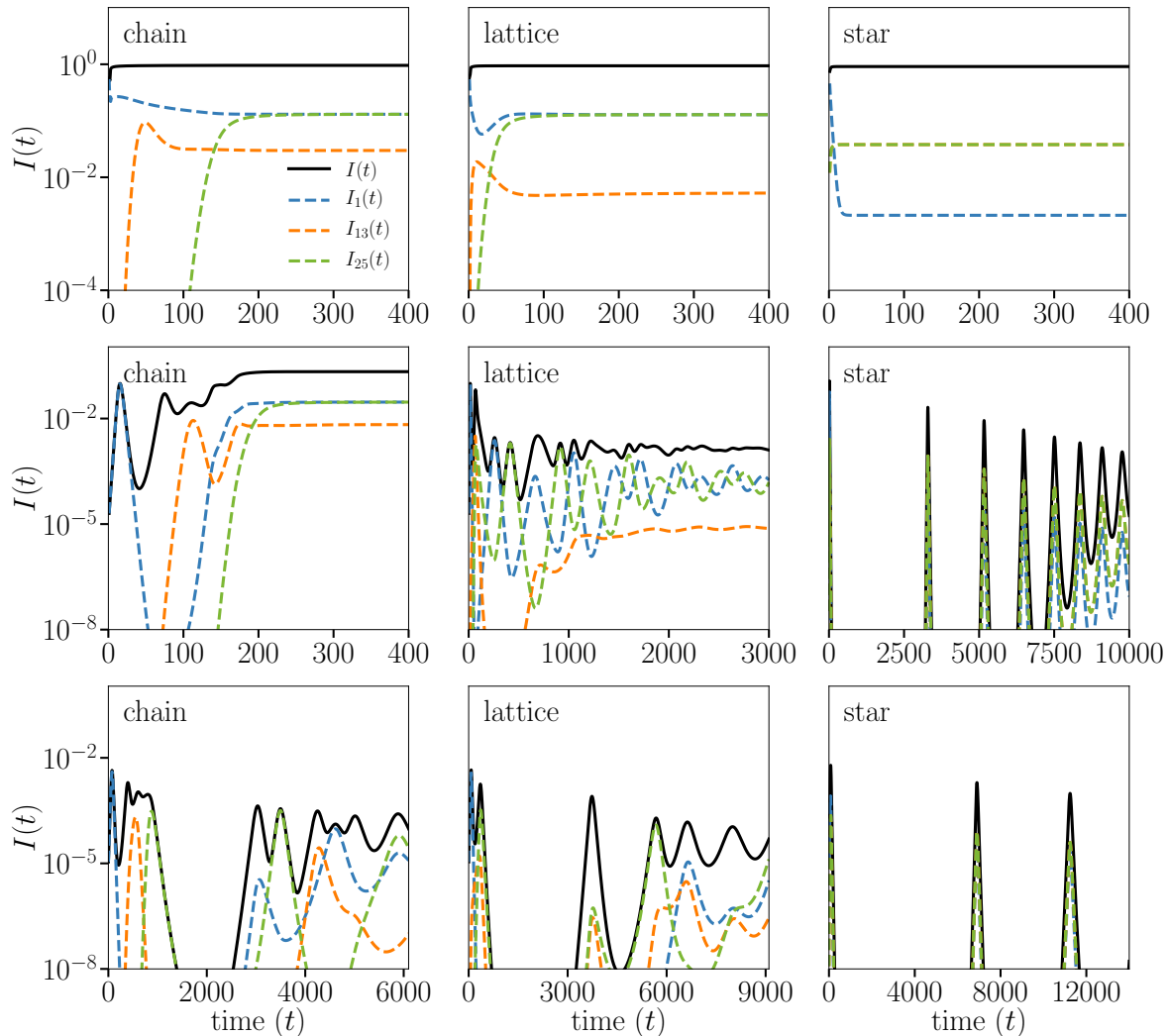


Figure 5. Integration of the ODEs on three toy genotype networks — the chain (left column), square lattice (middle column) and star (right column) — all with 25 strains. We fix the recovery rate $\gamma = 1$, the mutation rate $\mu = 1/1000$, the waning immunity rate $\alpha = 1/5000$ and the transcending immunity $\Delta = 4$ and vary the transmission rate: $\beta = 25$ (**top**), $\beta = 1.7$ (**middle**), $\beta = 1.1$ (**bottom**). The system is initialized with a small fraction 10^{-5} of infections on an “end strain” (end for the chain, corner for the lattice, leaf for the star). On the chain we see successive activation of all strains, with the system stabilizing once the entire network is explored and evolution reaches a dead-end. The star sees cycles, caused by activation of the leaf strains. The lattice is much more interesting, with loops causing a random-like succession of strains to cycle. The dynamics become more interesting for the bottom row, with transmission rates between the epidemic and immune invasion thresholds, with cycles and chaos-like dynamics. The closer we get to the true epidemic thresholds $\beta_c = 1$, the longer the interesting transient dynamics.

values decrease by orders of magnitude. In practice, this shows that any finite size simulations of the dynamics captured by our model would likely lead to strain extinction, with potential to reemerge through mutations. Discrete events are unfortunately not captured in ODE models as they assume continuous values, or infinite population.

4 Conclusion

The introduction of an underlying genotype network to a multistrain model has demonstrated the emergence of cyclicity, infection localization, and sequential phase transitions, all in one model. Simple mathematical arguments have allowed us to solve for the transitions observed and highlight the nontrivial impact of the structure of the genotype network. Rich infection dynamics are seen between the epidemic threshold and the immune invasion threshold. Altogether, what these results show is that many features of infectious disease dynamics often explained by environmental factors or host behaviour, such as cyclicity³⁰, unpredictability³¹ and sequential transitions³², can also be explained by adding a layer of biological complexity in the form of a genotype network. Our results thus highlight the importance of going beyond the “one disease, one pathogen” paradigm, with complex dynamics emerging from even the most simple genotype network structures.

Future work needs to be done to integrate this modelling approach with real genomic data. Likewise, the interplay of our results with the finite size and the contact structure of the host population needs to be investigated; as does the role of strain extinction and emergence. Different modelling approaches will need to be considered, such as explicitly modeling the growth and evolution of the genotype network as it co-evolves (albeit on a different timescale) with the spread of the infectious disease in the host population. Coupling the large modeling literature on growing networks³³ with that of network epidemiology²⁹ should lead to a richer understanding of how networks, both biological and social, impact epidemics. Finally, this type of models could also be appropriate to re-imagine vaccination strategies. The literature on targeted immunization and influential spreaders on networks could then be leveraged^{34–37}, but rather than targeting central individuals the objective would be to best hinder and block the immune evasion of the pathogen as it mutates along its genotype network.

In terms of applying these models to specific scenarios, there is a need for unbiased pathogen genomic data, as well as an understanding of their antigenic properties, to inform models that account for these features using real-world data and to refine the cross-protective immune effects between strains of a pathogen. Similarly, we need more realistic models to take advantage of the growing body of genomic data available and refine the mechanisms driving mutation and immunity. We call for the refinement of immune mechanisms and immune history to allow their incorporation in mathematical disease models. Further understanding of how pathogens explore genotype space, the growth of genotype networks, the role of host immunity towards past strains, and the influence of the above on the fitness landscape of pathogens will better inform models incorporating multiple strains, cross-protective effects, and evolution of a pathogen.

References

1. Meiklejohn, G. & Bruyn, H. B. Influenza in California during 1947 and 1948. *Am. journal public health nation's health* **39**, 44–49, DOI: [10.2105/ajph.39.1.44](https://doi.org/10.2105/ajph.39.1.44) (1949).
2. Sanjuán, R., Nebot, M. R., Chirico, N., Mansky, L. M. & Belshaw, R. Viral mutation rates. *J. Virol.* **84**, 9733–9748, DOI: [10.1128/JVI.00694-10](https://doi.org/10.1128/JVI.00694-10) (2010). <https://jvi.asm.org/content/84/19/9733.full.pdf>.
3. de Jong, J. C. *et al.* Antigenic and genetic evolution of swine influenza A (H3N2) viruses in Europe. *J. Virol.* **81**, 4315–4322, DOI: [10.1128/JVI.02458-06](https://doi.org/10.1128/JVI.02458-06) (2007). <https://jvi.asm.org/content/81/8/4315.full.pdf>.
4. Flannery, B. *et al.* Early estimates of seasonal influenza vaccine effectiveness - United States, January 2015. *MMWR Morb. mortality weekly report* **64**, 10–15 (2015).
5. Flannery, B. *et al.* Interim estimates of 2016-17 seasonal influenza vaccine effectiveness - United States, February 2017. *MMWR Morb Mortal Wkly Rep* **66**, 167–171, DOI: [10.15585/mmwr.mm6606a3](https://doi.org/10.15585/mmwr.mm6606a3) (2017).
6. Flannery, B. *et al.* Interim estimates of 2017-18 seasonal influenza vaccine effectiveness - United States, February 2018. *MMWR Morb Mortal Wkly Rep* **67**, 180–185, DOI: [10.15585/mmwr.mm6706a2](https://doi.org/10.15585/mmwr.mm6706a2) (2018).
7. Doyle, J. D. *et al.* Interim estimates of 2018-19 seasonal influenza vaccine effectiveness - United States, February 2019. *MMWR Morb Mortal Wkly Rep* **68**, 135–139, DOI: [10.15585/mmwr.mm6806a2](https://doi.org/10.15585/mmwr.mm6806a2) (2019).
8. Gilchuk, I. *et al.* Cross-neutralizing and protective human antibody specificities to poxvirus infections. *Cell* **167**, 684–694.e9 (2016).
9. Hensley, L. E. *et al.* Demonstration of cross-protective vaccine immunity against an emerging pathogenic Ebolavirus species. *PLoS pathogens* **6**, e1000904–e1000904 (2010).
10. Epstein, S. L. & Price, G. E. Cross-protective immunity to influenza A viruses. *Expert. Rev. Vaccines* **9**, 1325–1341 (2010).
11. Peeters, B. *et al.* Genetic versus antigenic differences among highly pathogenic H5N1 avian influenza A viruses: Consequences for vaccine strain selection. *Virology* **503**, 83 – 93, DOI: <https://doi.org/10.1016/j.virol.2017.01.012> (2017).
12. Halstead, S. B. Neutralization and antibody-dependent enhancement of dengue viruses. *Adv Virus Res* **60**, 421–467 (2003).

13. Katzelnick, L. C. *et al.* Antibody-dependent enhancement of severe dengue disease in humans. *Science* **358**, 929–932, DOI: [10.1126/science.aan6836](https://doi.org/10.1126/science.aan6836) (2017). <https://science.sciencemag.org/content/358/6365/929.full.pdf>.
14. Kucharski, A. V. . G. J. R., A. J. Capturing the dynamics of pathogens with many strains. *J. mathematical Biol.* **72**(1-2), 1–24, DOI: <https://doi.org/10.1007/s00285-015-0873-4> (2016).
15. Ferguson, N. & Andreasen, V. The influence of different forms of cross-protective immunity on the population dynamics of antigenically diverse pathogens. In Castillo-Chavez, C., Blower, S., van den Driessche, P., Kirschner, D. & Yakubu, A.-A. (eds.) *Mathematical Approaches for Emerging and Reemerging Infectious Diseases: Models, Methods, and Theory*, 157–169 (Springer New York, New York, NY, 2002).
16. Kucharski, A. J. & Gog, J. R. Age profile of immunity to influenza: effect of original antigenic sin. *Theor Popul Biol* **81**, 102–112 (2012).
17. Kamo, M. & Sasaki, A. The effect of cross-immunity and seasonal forcing in a multi-strain epidemic model. *Phys. D: Nonlinear Phenom.* **165**, 228 – 241 (2002).
18. Minayev, P. & Ferguson, N. Improving the realism of deterministic multi-strain models: implications for modelling influenza A. *J. The Royal Soc. Interface* **6**, 509–518 (2009).
19. Feng, Z. & Velasco-Hernández, J. X. Competitive exclusion in a vector-host model for the dengue fever. *J. mathematical biology* **35**, 523–544 (1997).
20. Wagner, A. A genotype network reveals homoplastic cycles of convergent evolution in influenza A (H3N2) haemagglutinin. *Proc. Royal Soc. B: Biol. Sci.* **281**, 20132763, DOI: [10.1098/rspb.2013.2763](https://doi.org/10.1098/rspb.2013.2763) (2014). <https://royalsocietypublishing.org/doi/pdf/10.1098/rspb.2013.2763>.
21. Girvan, M., Callaway, D. S., Newman, M. E. & Strogatz, S. H. Simple model of epidemics with pathogen mutation. *Phys. Rev. E* **65**, 031915 (2002).
22. Uekermann, F. & Sneppen, K. Spreading of multiple epidemics with cross immunization. *Phys. Rev. E* **86**, 036108 (2012).
23. Lipsitch, M., Cohen, T., Murray, M. & Levin, B. R. Antiviral resistance and the control of pandemic influenza. *PLoS Med* **4**, e15 (2007).
24. Hébert-Dufresne, L., Patterson-Lomba, O., Goerg, G. M. & Althouse, B. M. Pathogen mutation modeled by competition between site and bond percolation. *Phys. review letters* **110**, 108103 (2013).
25. Althouse, B. M., Patterson-Lomba, O., Goerg, G. M. & Hébert-Dufresne, L. The timing and targeting of treatment in influenza pandemics influences the emergence of resistance in structured populations. *PLoS Comput. Biol* **9**, e1002912 (2013).
26. Patterson-Lomba, O., Althouse, B. M., Goerg, G. M. & Hébert-Dufresne, L. Optimizing treatment regimes to hinder antiviral resistance in influenza across time scales. *PloS one* **8**, e59529 (2013).
27. Gomes, M. G. M., Medley, G. F. & Nokes, D. J. On the determinants of population structure in antigenically diverse pathogens. *Proceedings. Biol. sciences* **269**, 227–233, DOI: [10.1098/rspb.2001.1869](https://doi.org/10.1098/rspb.2001.1869) (2002).
28. Kish, L. *Survey Sampling* (John Wiley & Sons, New York, 1965).
29. Pastor-Satorras, R., Castellano, C., Van Mieghem, P. & Vespignani, A. Epidemic processes in complex networks. *Rev. Mod. Phys.* **87**, 925–979, DOI: [10.1103/RevModPhys.87.925](https://doi.org/10.1103/RevModPhys.87.925) (2015).
30. Althouse, B. M. & Hébert-Dufresne, L. Epidemic cycles driven by host behaviour. *J. The Royal Soc. Interface* **11**, 20140575 (2014).
31. Scarpino, S. V. & Petri, G. On the predictability of infectious disease outbreaks. *Nat. communications* **10**, 1–8 (2019).
32. Allard, A., Althouse, B. M., Scarpino, S. V. & Hébert-Dufresne, L. Asymmetric percolation drives a double transition in sexual contact networks. *Proc. Natl. Acad. Sci.* **114**, 8969–8973 (2017).
33. Dorogovtsev, S. N. & Mendes, J. F. Evolution of networks. *Adv. physics* **51**, 1079–1187 (2002).
34. Pastor-Satorras, R. & Vespignani, A. Immunization of complex networks. *Phys. review E* **65**, 036104 (2002).
35. Cohen, R., Havlin, S. & Ben-Avraham, D. Efficient immunization strategies for computer networks and populations. *Phys. review letters* **91**, 247901 (2003).
36. Hébert-Dufresne, L., Allard, A., Young, J.-G. & Dubé, L. J. Global efficiency of local immunization on complex networks. *Sci. reports* **3**, 2171 (2013).

37. Morone, F. & Makse, H. A. Influence maximization in complex networks through optimal percolation. *Nature* **524**, 65–68 (2015).